Int. J. Electron. Commun. (AEÜ) 137 (2021) 153826

Contents lists available at ScienceDirect

International Journal of Electronics and Communications

journal homepage: www.elsevier.com/locate/aeue

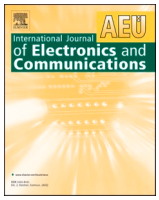

Regular paper

A comprehensive design analysis of a cost-effective WPT system with a class-E power amplifier and a T-matching network

Amir Fereshtian [a,*], Javad Ghalibafan [a], Mohsen Koohestani [b,c]

[a] Department of Electrical Engineering, Shahrood University of Technology, Shahrood, Iran
[b] Department of Electrical and Control Engineering, École Supérieure d'Électronique de l'Ouest (ESEO), Angers 49107, France
[c] Institut d'Électronique et de Télécommunications de Rennes (IETR), Université de Rennes 1, Rennes 35042, France

ARTICLE INFO

Keywords:
Wireless power transfer
Coupling coils
Class-E power amplifier
T-network

ABSTRACT

Magnetically-coupled resonant wireless power transfer systems (WPTs) operating in the megahertz range is well-suited for mid-range transmission of moderate power levels. The class-E power amplifier (PA) is attractive for the MHz WPT applications due to the high-efficiency and soft-switching properties. However, since the output power and the efficiency of the class-E PA strongly depends on the output load, any change in the mutual inductance of coupling coils, which leads to the PA load variation, results in a dramatic loss in the overall performance of WPT system. This paper provides a comprehensive design analysis to analytically and numerically mimic the PA behavior to conveniently adapt any variation of the input impedance of the coupled coils to the PA optimum load using a T-type matching network. An equivalent circuit analysis followed by the design theory for the class-E PA, coupled coils, and the T-network has been presented. For validation purposes, the class-E PA implemented by the cost-effective IRF640 MOSFET was first fabricated and its performance was measured for different load values. The PA efficiency and output power was measured as high as 96.7% and 25.8 W, respectively, for the optimum load value of 9 Ω, which was closely predicted from the theory. A 1 MHz WPT system was then built for the operating range up to 27 cm, showcasing its behavior in presence and absence of the proposed T-type matching circuits at two arbitrary 10 cm and 25 cm distances between the coupling coils; the input impedance of the WPT system for those separation distances were 4 Ω and 0.2 Ω, respectively. Results demonstrate power transfer efficiencies of 88% and 15% at distances of 10 cm and 25 cm with the T-network, respectively, improved by 33% and 12% to the non-matching state, respectively. The overall DC output power achieved using a full-bridge rectifier are 21.9 W and 6.8 W at 10 cm and 25 cm, respectively.

1. Introduction

Recently, wireless power transmission (WPT) has attracted much attention not only in the consumer electronics market but also in automotive, medical, military [1]. With the current trend to wirelessly charge batteries, pioneering vehicle manufacturers as well as producers of cell phones, tablets, pacemakers, and etc. have been integrating this promising technology into their new products [2–4].

Well-known WPT techniques are inductive coupling, magnetic resonant coupling (MRC), microwave and laser [1]. With a compromise among operating frequency, transfer distance, coil dimensions, and the transmission power level, the MRC is more popular due to its ability to transfer power at a mid-range distance (up to a few meters) with moderate power levels (a few watts to hundreds of watts) [2]. In that method, the power is transferred via magnetic fields between transmitter (Tx) and receiver (Rx) coils that resonate at the same frequency. In MRC WPT systems, the operating frequency can be selected depending on the intended application. For example, the low-frequency operation such as 20–205 kHz is suitable for high power applications at short ranges (less than 20 cm) such as for electric vehicles battery charging in the kilowatt range [5,6]. The 6.78 and 13.56 MHz ISM bands are mostly appropriate for power transmission in the order of hundreds of watts over mid-range distances (up to a few meters) with more compact coil structure [7].

Another high-potential but less-common operating frequency for WPT applications is 1 MHz [8–13]. For a target application to wirelessly charge low power consumer electronics, that frequency has been adopted for the purpose of the study as (i) it would lead to decreased

* Corresponding author.
E-mail address: fereshtian.amir@gmail.com (A. Fereshtian).

https://doi.org/10.1016/j.aeue.2021.153826
Received 29 October 2020; Accepted 14 May 2021
Available online 20 May 2021

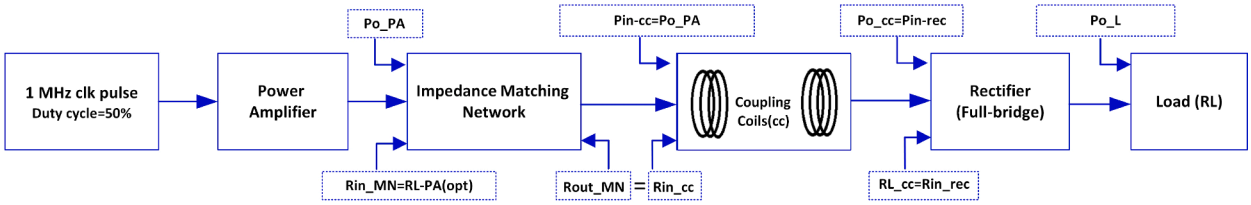

Fig. 1. Different parts of the WPT system including matching network.

switching losses and, consequently, high-efficiency operation with less technical difficulties in the PA fabrication process, and (ii) it would make it possible to employ cost-effective power transistors (such as IRF MOSFET) rather than costly GaN FETs commonly used for the MHz frequencies [14].

There has been a great deal of research for the design and optimization of WPT systems in a variety of areas, such as improvement of coupling coils [7,15], power amplifiers (PA) [16,17], load control [18–20] and multiband systems [21,22]. However, less attention has been paid to the role of the matching network between the PA and Tx coil and its direct impact on other parts of the system. The performance of the class-E PA is highly sensitive to the output load resistance, where the maximum efficiency occurs only for the optimum value. When the PA is connected to the coupled coils, any variation in the position of coils, which modifies the mutual inductance, changes the output load of PA leading to a rapid decrease in the system transfer efficiency. Therefore, despite the careful design for other parts, the use of a matching network is necessary to adapt the PA optimum load to that of the coupled coils for any distance between Tx/Rx coils.

Studies in [23,24], reported WPT systems with air-core transformer matching networks. In [11,25,26], the frequency tracking method was used for impedance matching. Other prevalent approaches implemented in WPT systems include the use of lumped-element matching networks such as L- and Π-type [17,27,28]. Π- and T-networks have not only a wider matchable region compared to L-types but also can get control of the circuit quality factor [29,30]. Since a T-type has never been implemented in the MHz WPT systems, it has been used for the purpose of the study. It is worth mentioning that (i) for a low output load value close to zero, a Π-network is much less effective compared to a T-type when designing the matching circuit using the Smith chart, and (ii) consisting of three component variables would allow a more reliable impedance matching capability compared to a L-type to easily control other criteria such as parasitic effects and harmonic rejection [30].

In [31], a soft-switching zero voltage switching (ZVS) based class-E PA and rectifier has been used. However, the system performance was only investigated in a constant coupling factor of $k = 0.1327$ between Tx/Rx coils. In [32], the input power of the kHz WPT system was provided by an inverter with four switches, which can be coslty particularly in the MHz range. A high-efficiency class-E PA with only one switch is more common in WPT applications [27,31]. In [32], an adaptive impedance matching was implemented in the receiver side. However, no matching network has been used in the Tx side caussing the significant power loss arised for different coils positions. In [17,27], the class-E PA and rectifier as well as the Π configuration matching network were employed in the Tx side. However, the study in [33] demonstrated that, similar to the class-E rectifier, the full-bridge rectifier can lead to achieve comparable AC-to-DC efficiency (as high as 90%) but with fewer complications in the design process. Therefore, the current study benefits from the full-bridge rectifier with fast switching Schottky diodes.

A comprehensive design analysis has been performed to analytically and numerically mimic the ZVS class-E PA behavior, monitoring its performance separately from the WPT system for different load values. An equivalent circuit analysis followed by the design theory of the class-E PA, coupled coils, and the T-network has been presented. For validation purposes, a full WPT system was fabricated and a demonstration experiment to wirelessly light up a 3 W LED at a separation distance 1.6 times larger than the outer diameter of the coils (i.e. 15 cm) was presented.

2. WPT System Design and Analysis

Fig. 1 demonstrates all parts of the MCR WPT system. As shown in this figure a clock pulse with 50% duty cycle was used to drive the MOSFET of PA. The PA converts the DC input power to the AC output power and then delivers to the load resistance ($R_{L_{-PA}}$). The maximum efficiency of the PA can be obtained only for a single value of load resistance that is called the optimum load, $R_{L_{-PA(opt)}}$. In practical WPT systems, when the coupled coils are connected to the PA, there is no external resistor for the PA and in fact the input resistance of the coupled coils ($R_{in_{-cc}}$) can be considered as the PA load. Therefore, $R_{L_{-PA}}$ is constantly changing when the positions of the two coils change leading to impedance mismatch between the PA and the coupled coils. An appropriate matching network is hence necessary to possibly achieve $R_{in_{-cc}} = R_{L_{-PA(opt)}}$.

In the next step, the AC output power of the PA is transferred through the magnetic fields between Tx/Rx coils, and then converted by the full-

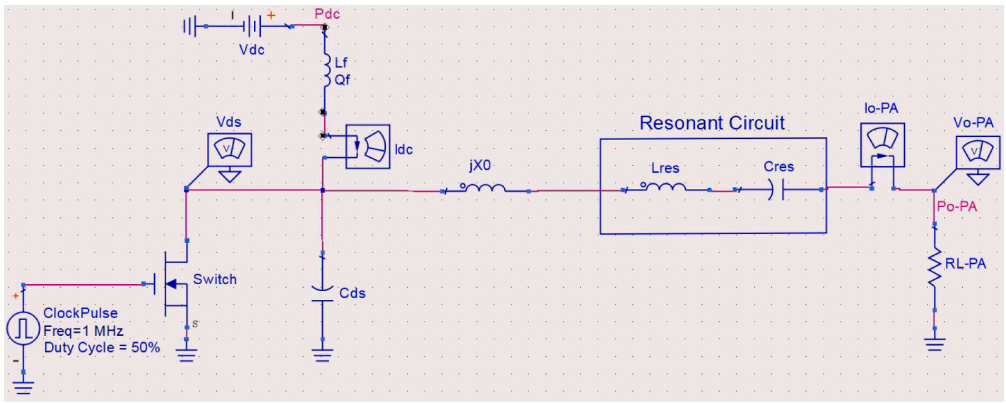

Fig. 2. Schematic of the class-E RF ZVS PA.

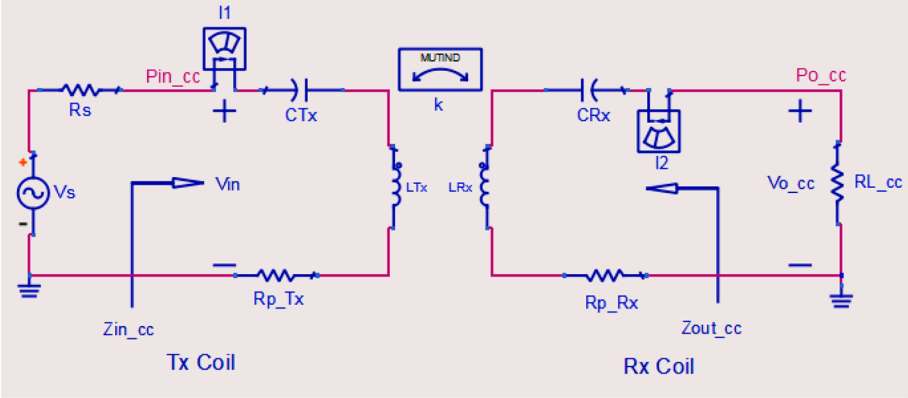

Fig. 3. Equivalent circuit model of the magnetically coupled coils.

bridge rectifier to DC power and delivered to the resistive load (R_L). According to [33], at 1 MHz operating frequency and for load resistors smaller than 50 Ω, the input resistance of full-bridge rectifier is almost linearly proportional to the load resistance while the negative input reactance is negligible. This condition simplifies the design of the receiver section and eliminates the need for adjusting the receiver capacitor to remove the negative reactance of the rectifier. The design steps of the class-E PA, coupled coils, and the matching network will be explained hereafter. Note that the analytical model developed in the study was implemented in Matlab, whereas the numerical simulations were conducted using the Keysight Advance Design System (ADS).

2.1. The Class-E ZVS PA Design Analysis

The initial concepts of the class-E power amplifier are not new and its mechanism has been well-documented in numerous studies (e.g. [16,34,35]). The conventional shape of zero voltage switching (ZVS) class-E PA was impelemented in ADS and is shown in Fig. 2. The MOSFET operates as a switch with an optimal duty cycle of 50%. $L_{res}/C_{res}$is a tuned filter to let only the first harmonic of the 1 MHz input frequency reach the load $R_{L_{\_PA}}$. The pure positive reactance jX_0 introduces the suitable phase shift between the switch and the output voltage to acquire the desired sinusoidal waveform. C_{ds} is the parallel capacitor in drain-source whereas L_f and Q_f are the inductor and quality factor of the radio frequency (RF) choke, respectively. I_{dc} and V_{dc} are the DC supply current and voltage of PA, respectively. The PA efficiency (also known as drain efficiency) is determined as the ratio of $P_{o_{\_PA}}$ and $P_{dc}, \eta_{\_PA} = P_{o_{\_PA}}/P_{dc}$ [17]. In order to maximize the PA efficiency, three key parameters of $R_{L_{\_PA(opt)}}, C_{ds}$ and X_0 should be carefully determined, which are given by the following Eqs. (1)–(3) [16,36]. Eqs. (4)–(7) represent the other required parameters for the optimal design. In those equations, $P_{o_{\_PA}}, f, \eta_{\_PA}$, and Q are the output power of PA, operation frequency, PA efficiency and the quality factor of the series resonant circuit, respectively.

$$R_{L_{\_PA(opt)}} = \frac{8}{\pi^2+4} \times \frac{V_{dc}^2}{P_{o_{\_PA}}} \tag{1}$$

$$C_{ds} = \frac{8}{\pi\omega R_{L_{\_PA(opt)}}(\pi^2+4)} \tag{2}$$

$$X_0 = \frac{\pi(\pi^2-4)}{16} R_{L_{\_PA(opt)}} \simeq 1.1525 R_{L_{\_PA(opt)}} \tag{3}$$

$$L_{res} = \frac{QR_{L_{\_PA(opt)}}}{\omega}, C_{res} = \frac{1}{\omega Q R_{L_{\_PA(opt)}}} \tag{4}$$

$$L_{f_{min}} = 2(\frac{\pi^2}{4}+1)\frac{R_{L_{\_PA(opt)}}}{f} \tag{5}$$

$$I_{dc} = \frac{P_{o_{\_PA}}}{\eta \times V_{dc}} \tag{6}$$

$$V_{ds} = 3.562 \times V_{dc} \tag{7}$$

2.2. The MRC Coils Design Analysis

Fig. 3 shows the equivalent circuit model for two magnetically coupled resonant coils. L_{Tx} and L_{Rx} are the inductance of Tx and Rx coils, respectively. $C_{Tx}$and $C_{Rx}$are the series capacitors to set the resonant frequencies of the coils. $Rp_{\_Tx}$ and $Rp_{\_Rx}$ are the parasitic resistance of Tx and Rx resonators, respectively. $R_{L_{\_cc}}$ is the load resistance of the coupling coil. V_s and R_s are the source voltage and resistance, respectively. Applying the Kirchhoff voltage law results in the following matrix equation:

$$\begin{bmatrix} V_s \\ 0 \end{bmatrix} = \begin{bmatrix} Z_{11} & Z_{12} \\ Z_{21} & Z_{22} \end{bmatrix} \begin{bmatrix} I_1 \\ I_2 \end{bmatrix} \tag{8}$$

where the impedance parameters at resonant frequency, $\omega_0 = 1/\sqrt{L_{Tx}C_{Tx}} = 1/\sqrt{L_{Rx}C_{Rx}}$, can be simplified and expressed as follows:

$$\begin{aligned} Z_{11} &= R_s + Rp_{\_Tx} \\ Z_{12} = Z_{21} &= j\omega M \\ Z_{22} &= R_{L_{\_cc}} + Rp_{\_Rx} \end{aligned} \tag{9}$$

where M is the mutual inductance between coils that is related to the coupling coefficient by [37.38]:

$$k = \frac{M}{\sqrt{L_{Tx}L_{Rx}}}, 0 \leqslant k \leqslant 1 \tag{10}$$

By substituting (9) in (8) and further simplification, the voltage transfer function (the ratio of $V_{O_{_cc}}$to V_S) can be expressed as the following:

$$\frac{V_{O_{\_cc}}}{V_S} = \frac{i\omega k\sqrt{L_{Tx}L_{Rx}}R_{L_{\_cc}}}{\omega^2 k^2 L_{Tx}L_{Rx} + (R_s + R_{p_{\_Tx}})(R_{L_{\_cc}} + R_{p_{\_Rx}})} \tag{11}$$

The power transfer efficiency of coupling coils can be written as [22,23]:

$$\eta_{\_cc} = \frac{P_{O_{\_cc}}}{P_{in_{\_cc}}} = (2\frac{V_{O_{\_cc}}}{V_S}(\frac{R_s}{R_{L_{\_cc}}})^{1/2})^2 \tag{12}$$

The critical coupling is the other key parameter that is defined as the coupling coefficient where the impedance matching and the maximum efficiency take place at the same time. To extract this parameter, the derivative of (11) is taken with respect to k. Setting the result equal to

zero and solving for k yield (13) [39]:

$$k_c = \sqrt{\frac{(R_s + R_{p\_Tx})(R_{L\_cc} + R_{p\_Rx})}{\omega^2 L_{Tx} L_{Rx}}} \tag{13}$$

where k_c is the critical coupling. At resonant frequency, the input impedance of the coupling coils ($Z_{in} = V_{in}/I_1 = V_S\text{-}R_S I_1/I_1$) is simplified as [23]:

$$Z_{in\_cc} = R_{in\_cc} = R_{p\_Tx} + \frac{\omega^2 k^2 L_{Tx} L_{Rx}}{R_{L\_cc} + R_{p\_Rx}} \tag{14}$$

In order to achieve the maximum achievable efficiency, the input impedance $Z_{in\_cc}(=R_{in\_cc})$ should be matched to R_s. By substituting (13) in (14), simplification and regardless of negligible parasitic resistance of the Tx coil with respect to the source resistance ($R_{p\_Tx} \ll R_s$), it is evident that the matching condition is satisfied at the critical coupling (k_c) and the input impedance equals the source resistance ($Z_{in\_cc} = R_s$). It should be noted that in (14) the load of coupled coils is considered as real form, R_{L_cc}, and it is identical to the input resistance of the full-bridge rectifier (Fig. 1). In [33], it has been demonstrated that selecting higher operating frequencies (such as 1 MHz and 6.78 MHz) with a wide range of load resistance in the full-bridge rectifier results in the negative input reactance and decreased system efficiency. To remove the negative input reactance, a compensation method such as tuning the series capacitor at the receiver resonator (C_{Rx}) can be used [33]. At 1 MHz, after eliminating the negative input reactance of the rectifier, the real part of its input impedance is almost linearly proportional to the load resistance. Moreover, when the load resistance is lower than 50 Ω, the negative input reactance of the rectifier is close to zero ($X_{in\_rec} \simeq 0$) without tuning the series capacitor of receiver coil. Therefore, since the load resistance of the full-bridge rectifier is considered lower than 50 Ω, the load impedance of the coupled coils is a pure resistor.

2.3. The Matching Network Design Analysis

After the successful design of the high-efficiency ZVS class-E PA with the optimum output resistance $R_{L\_PA(opt)}$ as well as the coupling coils with the input resistance of R_{in_cc}, the two following situations occur:

1. $R_{in\_cc} = R_{L\_PA(opt)}$: In this case, the system does not need the matching network and the Tx coil can be connected directly to the PA output. It should be noted that this situation happens only when the Tx and Rx coils are at a certain distance. In this condition, the whole output power of the PA is transferred to the coupled coils without any reflection and the system is expected to reach the maximum efficiency.
2. $R_{in\_cc} \neq R_{L\_PA(opt)}$: In this case (which usually takes place in practice), due to the mismatch, a considerable amount of output power of the PA is reflected and the system efficiency decreases dramatically. Two main factors that change R_{in_cc} and create the mismatch are the variation of Tx/Rx coil position and the load value of coupled coils.

In the current study, the methodology used to design the T-type matching network is to first extract the PA optimum load ($R_{L\_PA(opt)}$) as well as the input impedance of the coupled coils (R_{in_cc}) for the considered separation distances between the Tx/Rx coils. The proper T-type matching circuit elements are then selected depending on the $R_{L\_PA(opt)}$ value being lower or higher than the R_{in_cc} (see more details in subSection 3.3).

3. Simulation Results

This section deals with the simulation results for each part of the designed WPT system, i.e. the class-E PA, MRC coils, and the matching network.

Table 1
Calculated values of the PA elements from theory.

Parameter	value
$R_{L\_PA(opt)}$	11.5Ω
I_{dc}	1 A
V_{ds}	71.24 V
X_0	13.29
C_{res}	1.37 nF
L_{res}	18.3 μH
C_{ds}	2.53 nF
$L_{f(min)}$	80 μH

3.1. The Class-E ZVS PA

From (1), by specifying V_{dc} and the desired output power of P_{O_PA}, the value of $R_{L\_PA(opt)}$, the value of $R_{L\_PA(opt)}$ is calculated. Then, by choosing an appropriate Q (any value above 5 should suffice [36]) and η (here η = 100%) the rest of the circuit parameters can be obtained. For example, by setting $V_{dc} = 20$ V, $P_{O\_PA} = 20$ W, $f_0 = 1$ MHz, $\eta = 100\%$ and $Q = 10$, the PA circuit parameters are calculated and listed in Table 1.

Fig. 4a depicts the input and output power of the PA as a function of R_{L_PA}. It is evident that P_{O_PA} and DC input power P_{dc} cross each other at 11.5 Ω, which leads to achieve the maximum efficiency. For the optimal R_{L_PA} of 11.5 Ω, the value of output power obtained from the analytical and simulation closely match the initial desired value (20 W). Fig. 4b plots the efficiency obtained from the analytical and numerical analyses as a function of R_{L_PA}. As it can be seen, the maximum efficiency occurs for $R_{L\_PA} = 11.5$ Ω, which is in close agreement with the calculated value in Table 1. Furthermore, in a wide range from 5Ω to 24Ω the system is able to keep an efficiency as high as 90%. Referring to Fig. 4a, it should be pointed out that for values much lower than 11.5 Ω the enhancement of the DC input current I_{dc} significantly increases the DC input power P_{dc}, which can potentially damage the MOSFET or other elements in practice. Therefore, applying optimum resistance not only ensures the PA optimal performance but also satisfies the safety concerns.

Fig. 4c and 4d show the simulated PA characteristics as a function of the input power P_{in} for the optimum load value $R_{L\_PA} = 11.5\Omega$. Note that the power-added efficiency (PAE=P_{RFout}-P_{RFin}/P_{dc}), which takes into account the input RF power, was also reported [16,40]. As it can be seen, the PAE reaches its maximum at an input power of 22.5 dBm. The maximum output power and gain of the PA for that input power are 43.3 dBm and 20.8 dB, respectively.

Fig. 4e displays drain-source voltage V_{ds} for several different values of R_{L_PA} and also shows the gate pulse waveform with 50% duty cycle. As observed, only for R_{L_PA} the drain-source voltage V_{ds} becomes zero right before the transistor turns on satisfying ZVS codition and $dV_{ds}(\omega t)/d(\omega t) = 0$ (zero-derivative switching ZDS condition). The simultaneous realization of these conditions are called the soft-switching or optimum operation in which the PA has zero switching loss with the highest efficiency [16]. For other values of R_{L_PA} the system is in sub-optimum operation and the switching loss increases significantly [16]. Fig. 4f depicts the sinusoidal waveforms of the output voltage and current of the PA for the optimum load.

Since the quality factor of the choke inductor (Q_f) impacts the performance of the PA (the higher the quality factor the higher the PA efficiency), Fig. 5 depicts the PA efficiency as a function of the RF choke quality factor for various R_{L_PA}. As observed, while the maximum efficiency was achieved for the optimum load, the PA efficiency rises with the increase of the Q_f whatever the R_{L_PA}.

Fig. 6a plots the output voltage and current of the PA as a function of C_{ds} when $R_{L\_PA} = 11.5$ Ω. This figure illustrates the reasonable accuracy of the analytical method with the simulation model. Fig. 6b shows the output power of the PA versus C_{ds}. As observed the output power of the

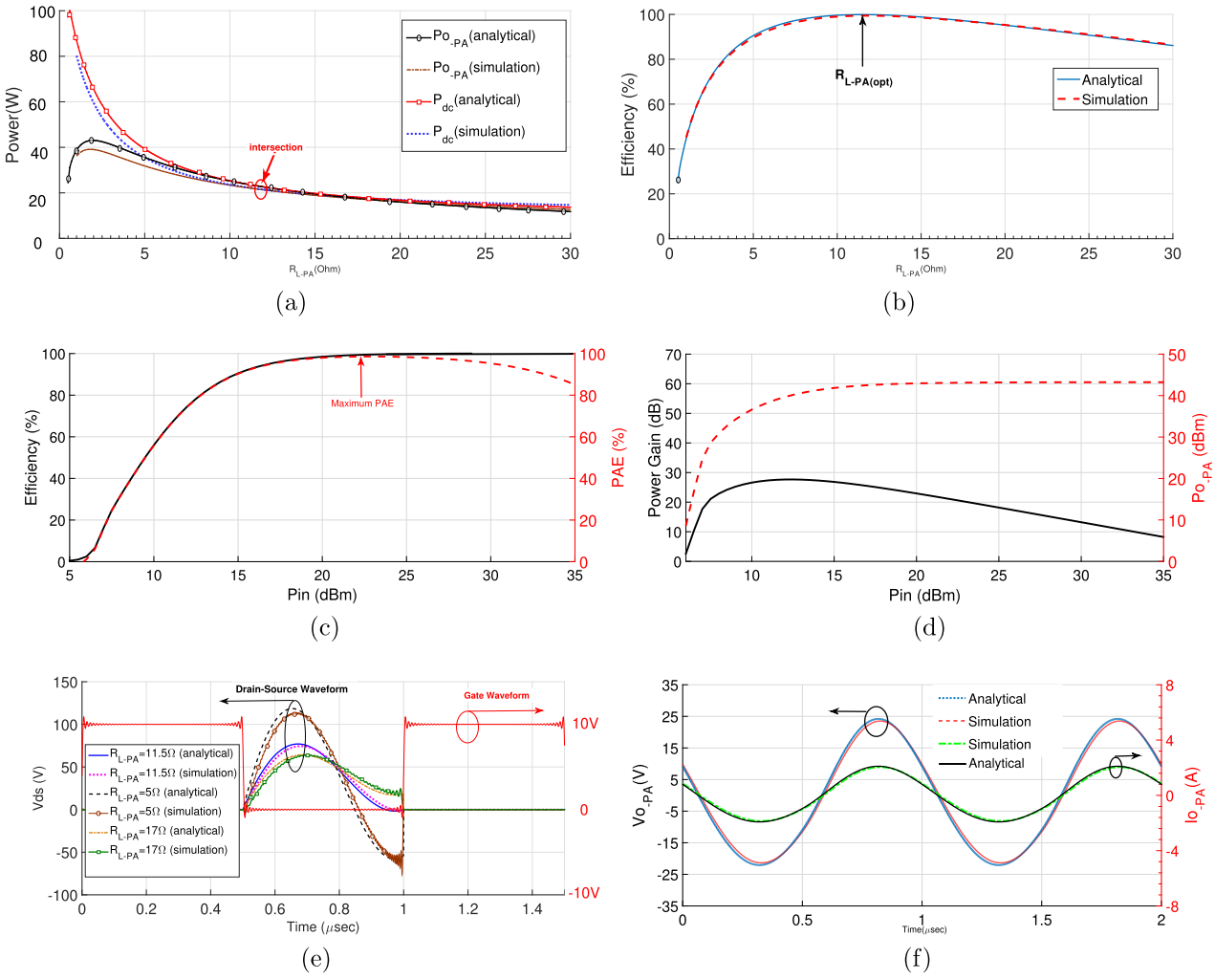

Fig. 4. Analytical and simulation results of the ZVS class-E PA. (a) output power and Dc input powe of the PA vs. R_{L_PA}; (b) efficiency vs. R_{L_PA}; (c) efficiency and power added efficiency vs. P_{in} for the optimum load value $R_{L\_PA(opt)}$; (d) power gain and output power vs. P_{in} for $R_{L\_PA(opt)}$; (e) drain-source voltage waveforms of the switch for different R_{L_PA}; (f) output voltage and current of the PA for $R_{L\_PA(opt)}$.

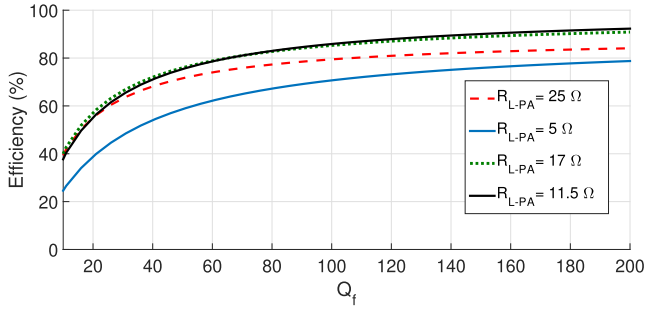

Fig. 5. The PA efficiency as a function of the RF choke quality factor Q_f for various R_{L_PA}.

PA for C_{ds} = 2.53 nF is close to the initial desired value (i.e. 20 W).

Fig. 7a and 7b display the V_{ds} versus C_{ds} (while R_{L_PA} = 11.5 Ω) and R_{L_PA} (while C_{ds} =2.53 nF), respectively. These figures show that for the values lower than the optimum one the drain-source voltage rises dramatically. Therefore, in order to avoid the risk of burning the MOSFET in practice, a MOSFET with the higher drain-source breakdown voltage compared to its optimum voltage (here $V_{ds(opt)}$ = 73.5 V) has to be selected.

In order to better understand the role of the duty cycle on the PA performance, Fig. 8a depicts the efficiency and output power of the PA with the optimum load for various duty cycles. As observed, the maximum efficiency was obtained for a duty cycle of 50% due to satisfying the ZVS and ZDS conditions. Moreover, the simulated output power at the optimum duty cycle is close to the initially defined value of 20 W. Fig. 8b shows the PA efficiency versus R_{L_PA} for three different duty cycle values. As it can be seen, the R_{L_PA} value corresponding to the maximum achievable efficiency varies depending on the duty cycle value; the maximum efficiency was attained only for the R_{L_PA} = 11.5 Ω and duty cycle = 50%. For other duty cycles, the PA is unable to reach the highest efficiency level (due to the sub-optimum operation) even for the load resistances corresponding to the maximum efficiency.

3.2. The MRC Coils

Fig. 9 shows the real part of the input impedance for the equivalent circuit model of coupled coils versus coupling coefficient (k) for four different values of R_{L_cc}, while L_{Tx}(=L_{Rx})=20 μH, C_{Tx}(=C_{Rx})=1.26 nF, R_{P_Tx}(=R_{P_Rx})=0 (assuming there is no parasitic resistance). In all cases, it is apparent that when the coupling coefficient increases, the real part of the input impedance increases significantly, which was previously verified by Eq. (14). Moreover, the lower R_{L_cc} leads to higher value for Re(Z_{in_cc}). Since both coils are resonant, the imaginary part of input

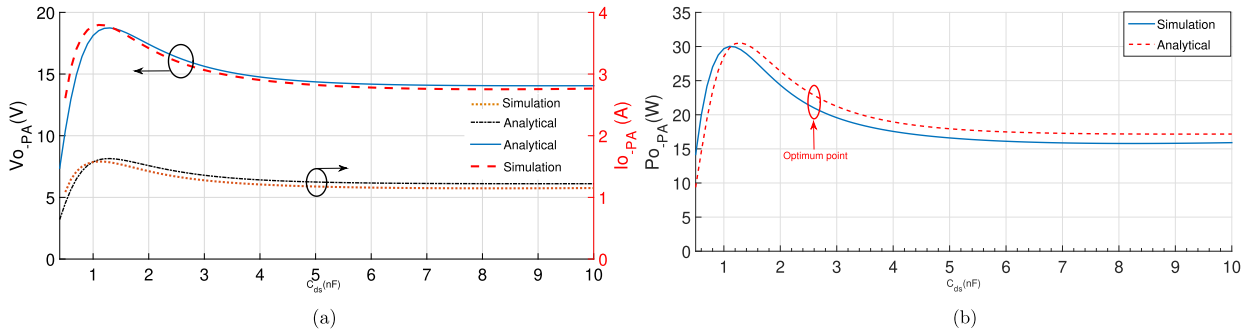

Fig. 6. The PA output results versus C_{ds}. (a) output current and voltage. (b) output power.

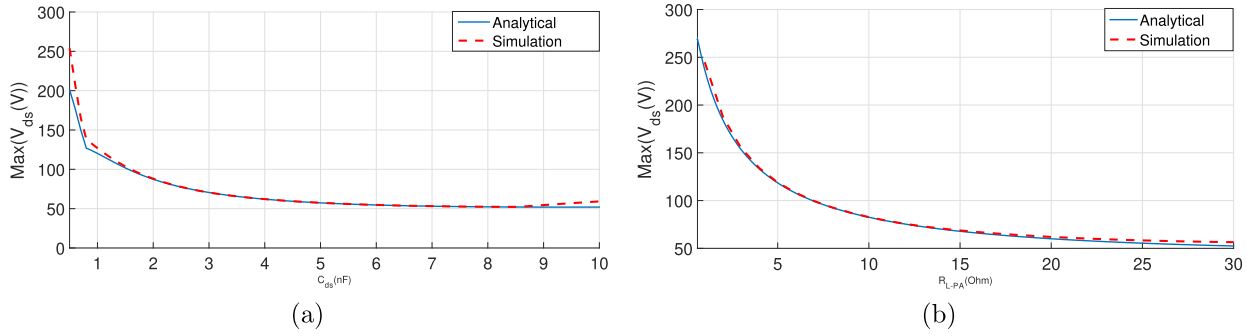

Fig. 7. Maximum drain-source voltage of the PA versus (a) C_{ds} and (b) R_{L_PA}.

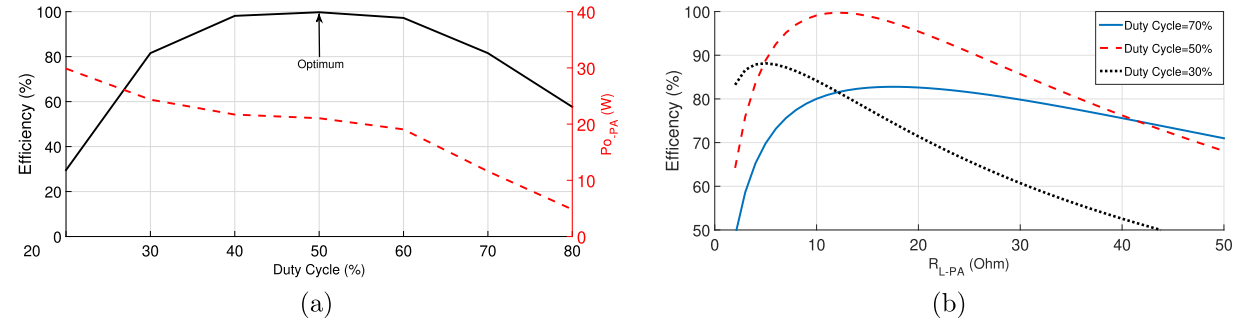

Fig. 8. (a) Efficiency and output power of the PA as a function of duty cycle for the optimum load value $R_{L\_PA(opt)}$; (b) efficiency as a function of R_{L_PA} for different duty cycle values.

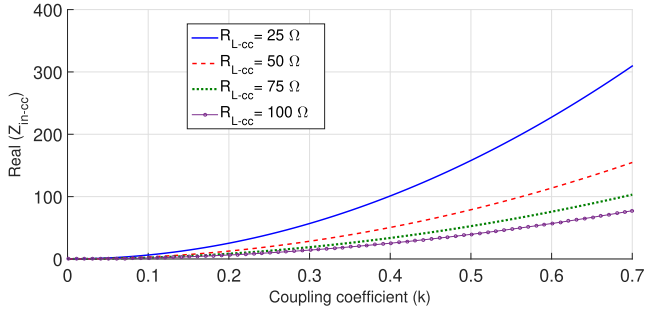

Fig. 9. The real part of the input impedance versus coupling coefficient for different R_{L_cc} values.

impedance is zero, Im(Z_{in_cc})=0.

For a clearer understanding, Fig. 10 illustrates the 3D curves of the efficiency as a function of frequency and coupling coefficient, where the source resistance is fixed at 50 Ω and three different values of 5 Ω (case 1), 50 Ω (case 2) and 100 Ω (case 3) are considered for the load resistance. In all cases, the maximum efficiency occurs in the critical coupling point (k_c) that is indicated by the red arrow. For coupling coefficients higher than the critical coupling point (k> k_c, so called the over-coupled state [24]) the frequency splitting occur and the efficiency significantly decreases at the operating frequency of 1 MHz. On the other hand, when the coupling coefficient is lower than the critical coupling point (k< k_c, so called the under-coupled state [24]) the efficiency begins to drop significantly while no frequency splitting happens. To sum up, for a fixed R_s value of 50 Ω, the critical coupling value increases with the increase of the R_{L_cc}, in line with Eq. (13). Therefore,

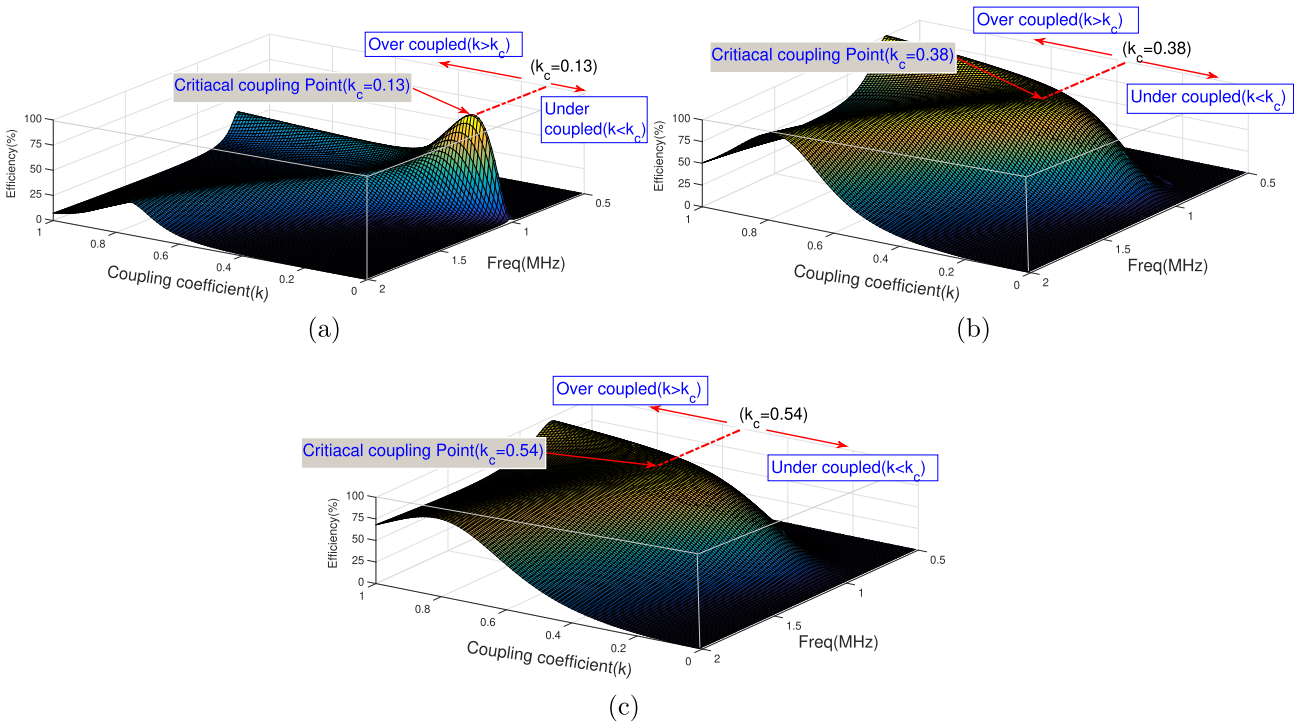

Fig. 10. 3D curve of the efficiency as a function of frequency and coupling coefficient for three different $R_{L_{cc}}$ values. (a) case 1: $R_{L_{cc}} = 5\ \Omega$. (b) case 2: $R_{L_{cc}} = 50\ \Omega$. (c) case 3: $R_{L_{cc}} = 100\ \Omega$.

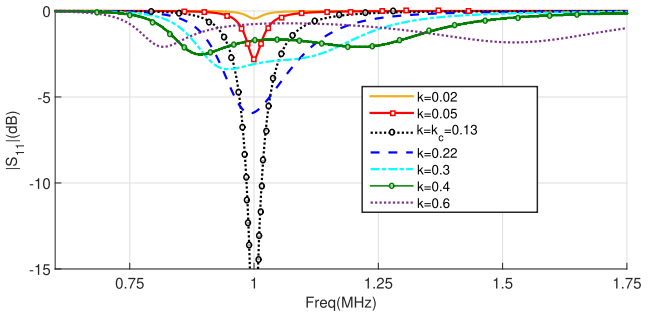

Fig. 11. Input reflection coefficient for various coupling coefficients (k) in case 1.

maximum matching and efficiency are achievable for shorter distances between the Tx/Rx coils by increasing the $R_{L_{cc}}$ value.

Fig. 11 shows the input reflection coefficient of case 1 ($R_{L_{cc}} = 5\ \Omega$) versus frequency for various coupling coefficients. As observed, maximum matching condition takes place for $k{=}k_c = 0.13$, which is identical to the critical coupling point in Fig. 10a. Moreover, for $k > k_c$ the frequency splitting phenomenon gradually appears, whereas for $k < k_c$ the impedance mismatch increases significantly.

Since a constant value for the input resistance was so far considered, there was therefore no control over the coupling coefficient k_c that maximizes the efficiency. For each arbitrary coupling coefficient, the maximum efficiency can be achieved to a reasonable extent when the matching condition is satisfied. In Fig. 12 the input reflection coefficient and efficiency are plotted for case 1 versus R_s for four different coupling coefficients. As observed, for a higher value of k, a higher R_s is needed to achieve the impedance matching, as can be deduced from Eq. (14). Moreover, it can be concluded that there exists an exclusive and suitable R_s (and vice versa) for every coupling coefficient that leads to the perfect matching and maximized efficiency. According to the concepts and examples that have been expressed in this section, the impedance matching for the coupled coils is of uppermost importance to reach the optimal performance in the overall WPT system.

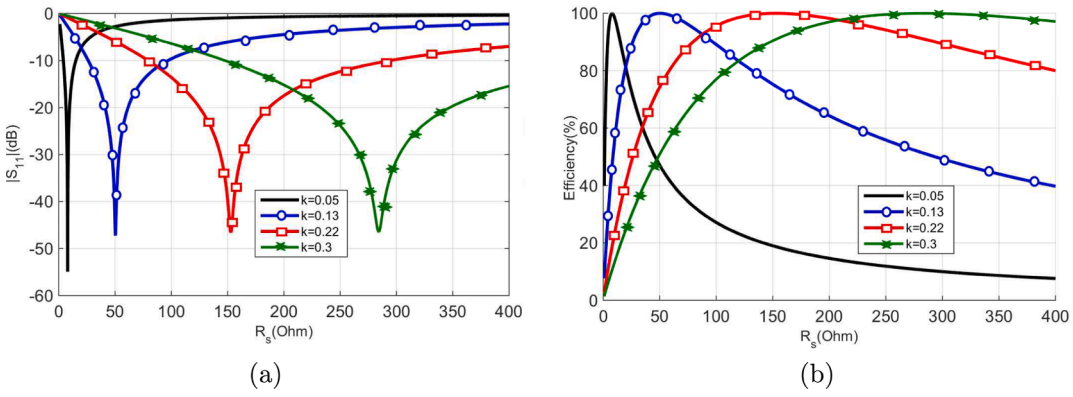

Fig. 12. Simulation results of case 1 ($R_{L_{cc}} = 5\ \Omega$) versus R_s for different coupling coefficient (k) values. (a) input reflection coefficient; (b) efficiency.

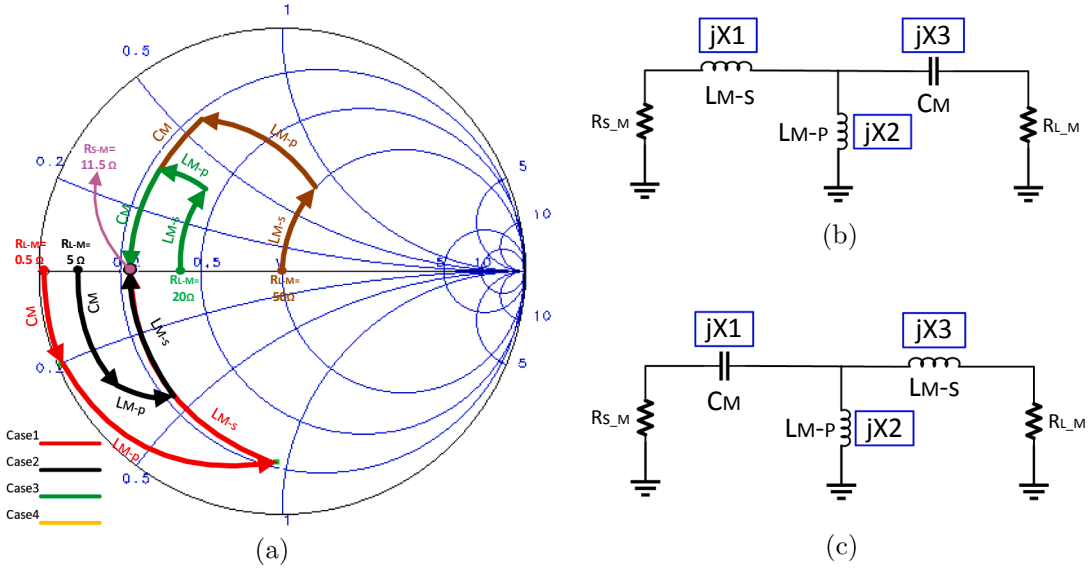

Fig. 13. (a) Impedance matching process using Smith chart for the considered cases; T-type matching networks for two states: (b) $R_{L\_M}<R_{S\_M}$(case 1 and 2). (c) $R_{L\_M}>R_{S\_M}$(case 3 and 4).

Table 2
T-matching network lumped elements values for the considered cases when $R_{S\_M} = 11.5\ \Omega$.

	$R_{L\_M}<R_{S\_M}$		$R_{L\_M}>R_{S\_M}$	
Parameter	$R_{L\_M} = 0.5\ \Omega$ case 1	$R_{L\_M} = 5\ \Omega$ case 2	$R_{L\_M} = 20\ \Omega$ case 3	$R_{L\_M} = 50\ \Omega$ case 4
C_M	16.48 nF	10.3 nF	8.47 nF	5.85 nF
L_{M_P}	1.93 μH	7 μH	11 μH	7.47 μH
L_{M_S}	7 μH	3.5 μH	3.33 μH	5.88 μH

3.3. The T-type Matching Circuit

The T-type impedance transformation network is shown in Fig. 13. The goal here is to determine X_1,X_2, and X_3 to ensure the load resistance of matching network, $R_{L\_M}(=R_{in\_cc})$ well-adapts the source resistance $R_{S\_M}(=R_{L\_PA_{(opt)}})$. The Smith chart was used to design the matching network (Fig. 13a), where the load/source resistance are normalized to $Z_0 = 50\ \Omega$ (being the characteristic impedance of system). We first assume that $R_{S\_M}(=R_{L\_PA_{(opt)}}) = 11.5\ \Omega$ (the value obtained from Section 3.1), whereas four different values are considered for $R_{L\_M}(=R_{in\_cc})$ such as 0.5 Ω (case 1), 5 Ω (case 2), 20 Ω (case 3), 50 Ω (case 4). Two conditions, i.e. $R_{L\_M}<R_{S\_M}$ and $R_{L\_M}>R_{S\_M}$ were investigated separately. If $R_{L\_M}<R_{S\_M}$, to move from the load to source resistance in the chart, we initially need a series capacitor followed by a parallel inductor and then a series inductor, as shown in Fig. 13a for case 1 and 2; the relevant matching network is shown in Fig. 13b. In contrast, if $R_{L\_M}>R_{S\_M}$, for moving from the load to source resistance, we need a series inductor, followed by a parallel inductor and a series capacitor, as shown for case 3 and 4 in the Smith chart with the corresponding matching network in Fig. 13c.

Table 2 summarizes the calculated values of the lumped elements for each of the considered cases. Note that the use of L-type matching network with only two lumped elements limits not only the selection of the inductor and capacitor with standard values but also the control of the other criteria such as the circuit quality factor, parasitic effects and harmonic rejection [30]. T- or Π-networks with three elements provides not only more freedom in practice to conveniently choose a wide range of values for the inductors and capacitors but also leading to wider matchable regions compared to L-networks [28–30]. Specifically, as seen in the Smith chart (Fig. 13a), one can easily change the length of the paths for each of the considered cases, which is a great advantage in practice for choosing various values of lumped components.

It is worth mentioning that, based on the Smith chart design, to adapt very low load impedances in the order of a few tenths of ohms to those of the source in the order of a few ohms, unlike a T-type matching network, designing a Π-type makes it very challenging to move from the load towards the source in Smith chart. In other words, selecting a first shunt element in the Π-type would lead to a very small SWR circle radius, which would ineffectually limit the movement towards the source. That issue would even get more complicated for the PA load values closer to the input impedance of the WPT system. As is the case in the current study, for a large separation distance between the coupled coils (e.g. 25 cm) the input impedance of the 1 MHz WPT system drops off to very low values (<0.5 Ω) whereas the PA optimum load is in the order of few ohms (9 Ω). Hence, inserting a T-type matching circuit is preferred to a Π-type between the WPT system and the PA.

Table 3
Measured parameters of the experimental WPT system.

Power amplifier	Coupling coils	Matching net1	Matching net2
		d = 10 cm	d = 25 cm
$R_{L\_PA} = 9\ \Omega$	$C_{Tx} = 3.3$ nF	-	-
$L_f = 1$ mH	$L_{Tx} = 7.7\ \mu$H	$C_M = 25$ nF	$C_M = 65$ nF
$C_{ds} = 3$ nF	$C_{Rx} = 3.3$ nF	$L_{M_S} = 1.2\ \mu$H	$L_{M_S} = 1.45\ \mu$H
$L_0 = 1.8\ \mu$H	$L_{Rx} = 7.74\ \mu$H	$L_{M_P} = 2.1\ \mu$H	$L_{M_P} = 0.46\ \mu$H

4. Experimental results

In order to experimentally validate what has been presented in previous sections, the overall WPT system including the class-E PA, coupling coils, T-type matching network, and the full-bridge rectifier were implemented.

A low-cost IRF640 MOSFET was used as a switch with the drain-source voltage breakdown of 200 V. A DSO-2070 oscilloscope and function generator (DC-70 MHz) was employed to generate a pulse with 50% duty cycle for the MOSFET gate. The output voltage of the generator was not sufficient to drive the IRF640 MOSFET requiring minimum 10 V. Therefore, an IC gate drive TC4427 was utilized as the MOSFET

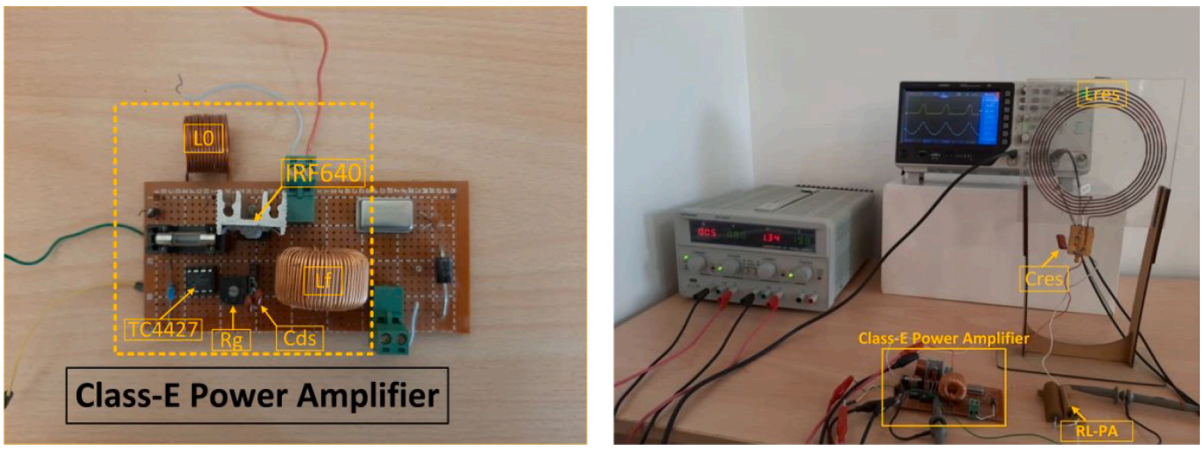

Fig. 14. Measurement setup to demonstrate the class-E PA performance.

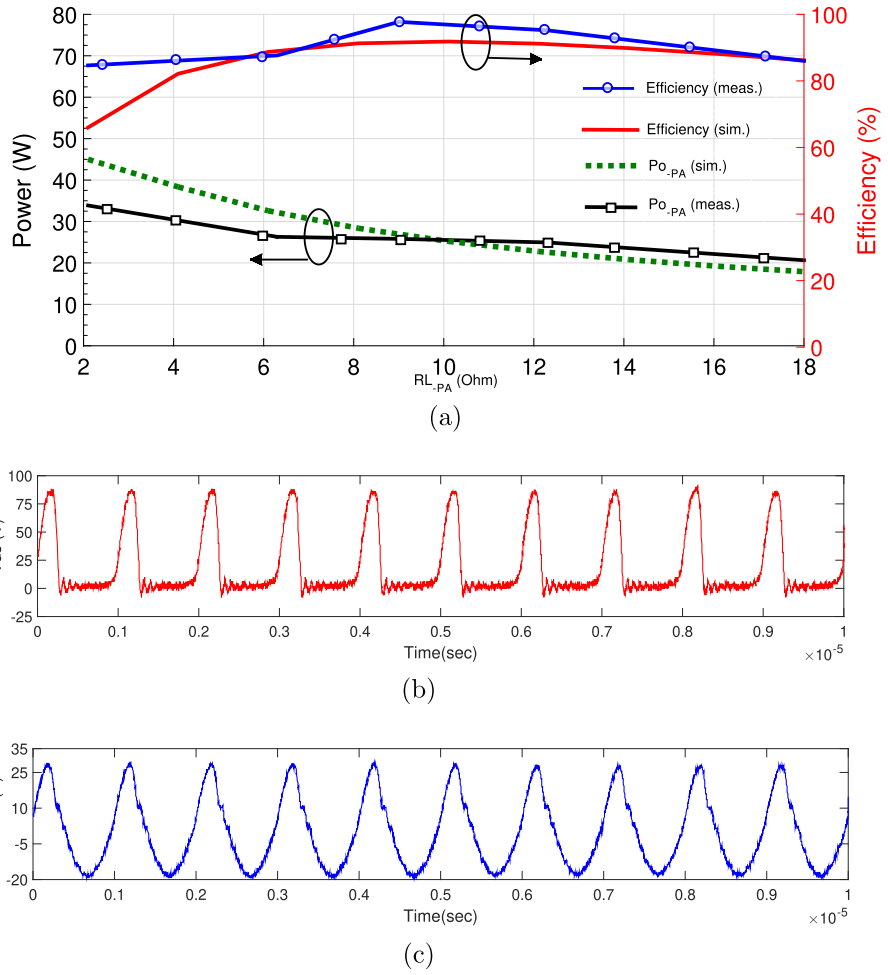

Fig. 15. (a) Simulated and measured results of the output power and efficiency of the PA versus R_{L_PA}; measured results of the (b) V_{ds} and (c) V_{o_PA} when $R_{L\_PA(opt)} = 9\ \Omega$.

driver to supply sufficient gate voltage. Moreover, a variable gate resistor (1–20 Ω) was considered to improve the MOSFET gate voltage waveform and decrease the switching loss. To assess the PA performance, a DC voltage of $V_{dc} = 20$ V was applied to the MOSFET drain, and the values of other components were obtained according to the required output power of $P_{o\_PA} = 25$ W, provided that $\eta_{\_PA} = 100\%$ and $Q = 5.4$. Note that by applying the theory provided in Section 2.1, the optimum R_{L_PA} value is 9.2 Ω. The specifications of the implemented circuit for the class-E PA and other sections are listed in Table 3.

Fig. 14 shows the fabricated experimental setup of the class-E PA to evaluate its performance individually. In the setup, the Tx coil is utilized as the resonant circuit. The measured and ADS simulated results of the efficiency and the output power of the PA were plotted in Fig. 15a as a function of R_{L_PA}. As observed, the efficiency reaches its maximum with $R_{L\_PA} = 9\ \Omega$, which is very close to the optimum value obtained from theory. Moreover, the measured PA maintains a high efficiency level (as

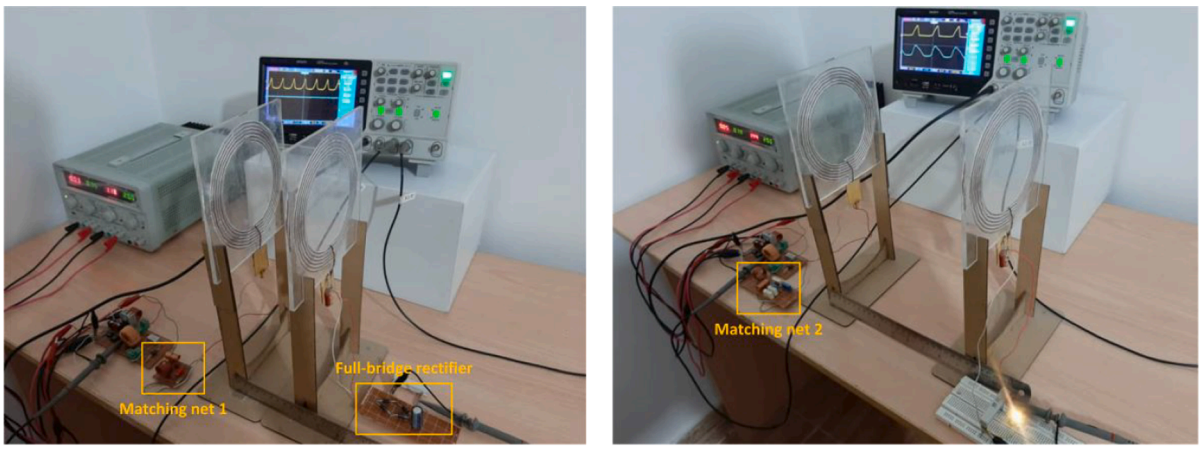

Fig. 16. The overall WPT system for two different distances in the presence of the proposed matching networks. (a) with rectifier and distance = 10 cm. (b) without rectifier and distance = 25 cm.

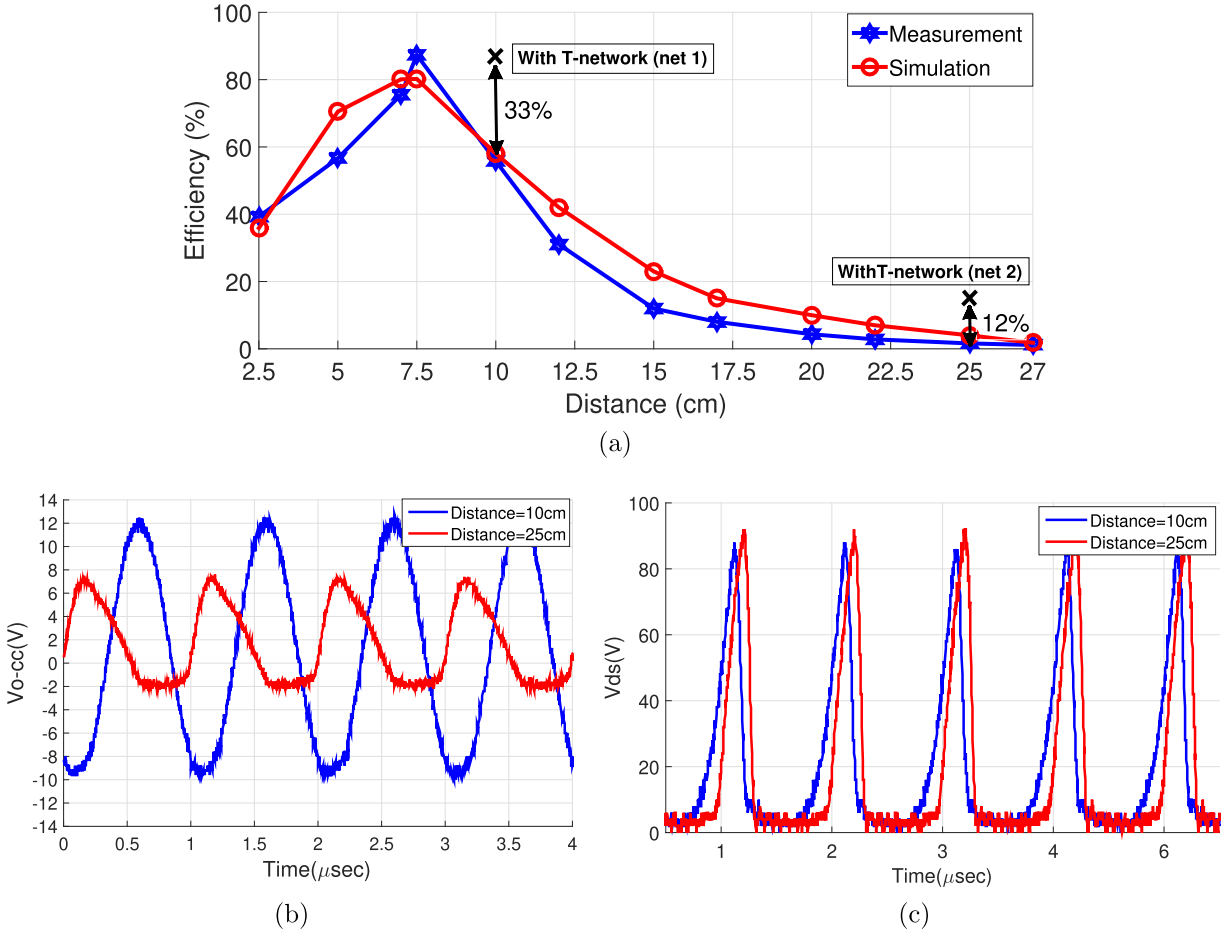

Fig. 17. (a) Measured and simulated efficiency as a function separation distances between the Tx/Rx coils in the absence of the matching network at 1 MHz; black crossed-lines indicate the measured efficiency in presence of the T-network at 10 cm and 25 cm; (b) measured output voltage of the coupled coils with the T-type matching network and (c) drain-source voltage of the PA for the two considered distances.

high as 90%) for a wide range of different load values from 7 to 16 Ω (6 to 14 Ω in simulations). Overall, a fairly good agreement was obtained between the simulated and measured results, especially for the higher compared to lower values of the load resistance. The latter can be related to the reduction of the MOSFET stability due to the significant increase of the DC input current of the PA for lower $R_{L_{-PA}}$ values. Fig. 15b and c display the measured drain-source voltage and the output voltage of the PA with $R_{L_{-PA_{(opt)}}} = 9$ Ω, respectively. The RMS value of the output voltage and power of the PA are 15.25 V and 25.8 W, respectively, being close to the desired values (15.18V and $P_{O_{-PA}} = 25$ W). The corresponding efficiency for that load is 96.7%, while the DC input power is $P_{dc} = 26.6$ W.

Table 4
State-of-the-art of WPT systems operating at 1 MHz.

Reference	Tx/Rx Coils type	Operating distance	Efficiency	Output power
[8]	Spiral diameter: 15 cm	7.5 cm	86%	4.4 W
[9]	Circular diameter: 10 cm	2.5 to 10 cm	< 11%	11 mW at 2.5 cm
[10]	Square spiral 40 × 40 mm^2	5 to 40 mm	< 41.2%	–
[11]	Circular diameter: 10 cm	Up to 20 cm	83% at 3 cm	25 W at 3 cm
			< 5% at > 10 cm	< 2 W at > 10 cm
[12]	Square plate 22.1 × 22.1 cm^2	Up to 2 mm	90.3% to 99.4%	9.3 to 9.94 W
[13]	Circular diameter: 10 cm	Up to 10 cm	< 87% up to 2.5 cm	< 7.9 W
			2.5% at 10 cm	
This work	Spiral diameter: 15 cm	Up to 27 cm	88% at 10 cm	18.1 W at 10 cm
			15% at 25 cm	4.1 W at 25 cm

Fig. 16 displays the experimental setup of the overall WPT system for two different distances. The Tx and Rx coils are identical with 5 turn and a 4 mm pitch, 15 cm outer diameter and 1.4 mm copper wire diameter. Plexiglases with a thickness of 5 mm and two wooden stands were used as the substrate and holders, respectively. In the rectifier part, four similar low-power-loss SR506 Schottky diodes were used.

In the measurement process, two arbitrary distances of 10 cm and 25 cm were selected between the Tx/Rx coils and the T-type matching network was implemented only in the Tx part to adapt the input resistance of coupling coils to the optimum PA load. Since the output resistance of the coupling coils Z_{out_cc} (i.e. 2.5 Ω and 0.9 Ω for 10 cm and 25 cm, respectively) were comparable to the chosen load value of 3.3 Ω, the use of the matching network was ignored in the Rx side. This is also valid for the case with the full-bridge rectifier as its input impedance (i.e. ∼ 1.7 Ω at 1 MHz according to Fig. 3a in [33]) is close to the selected load value.

Fig. 17a plots the measured and simulated efficiency (P_{O_cc}/P_{dc}) of the proposed WPT system in the absence of the rectifier as a function of distance between the Tx/Rx coils. A reasonably good agreement was obtained. As observed, the maximum efficiency occurs at 7.5 cm, which is the distance where the input resistance (seen from the coupling coils) becomes equal to the optimum resistance of the PA, i.e., $R_{in\_cc} = R_{L\_PA(opt)}$ = 9 Ω. Hence, at that distance the system reaches the best matching condition without using any matching network. For other distances between two coils, the use of the matching network is necessary to increase the overall system efficiency. The efficiency was measured in presence and absence of the matching network for two arbitrary distances between the Tx/Rx coils (Fig. 17a). As it can be seen, thanks to the T-type matching network, the efficiency at those distances was increased by 33% (from 55% to 88% at 10 cm) and 12% (3% to 15% at 25 cm). Moreover, based on the measured output voltages shown in Fig. 17b, the AC output power $P_{O\_cc}\left(=\frac{VO-cc^2_{rms}}{R_{L\_cc}}\right)$, at 10 cm and 25 cm were 18.1 W and 4.1 W, respectively.

It should be noted that the input resistances of the coupling coils (R_{in_cc}) for 10 cm and 25 cm at the resonant frequency of 1 MHz are 4 Ω and 0.2 Ω, respectively. For the two considered distances, since the input resistances of the coupled coils are lower than the $R_{L\_PA(opt)}$ = 9 Ω, the circuit model of Fig. 13b was selected and implemented as the matching network. As a showcase to light up a 3 W LED, the output load resistance was set to R_{L_cc} = 3.3 Ω, and with the AC output power of 4.1 W the system was able to successfully illuminate the LED at 25 cm distance (Fig. 16b). Without applying the matching network, the system efficiency was very low and the output power was less than 1 W, not being sufficient to light up the LED. Fig. 17c shows the measured drain-source voltage for the two considered distances. By applying the full-bridge rectifier, while R_L = 3.3 Ω, the overall efficiency (DC output power) at 10 cm and 25 cm separation distances are 93% (21.9 W) and 21.9% (6.8 W), respectively, where the overall efficiency is defined as (P_{O_L}/P_{dc}).

The characteristics of the WPT system developed in the current study were compared to those of the state-of-the-art operating at 1 MHz in terms of the operating range, efficiency and output power; a summary is provided in Table 4. As observed, taking into account the system dimensions and operating ranges, the transfer efficiency and output power of the systems decrease with the increase of the distance. However, at distances comparable to the overall dimensions of the coils the performance of the systems developed in the previous works degrades dramatically. Conversely, the obtained results of the proposed system demonstrate the suitability to operate at larger distances with fairly acceptable efficiency and output power levels.

5. Conclusion

A comprehensive design analysis of a 1 MHz WPT system including the class-E PA, coupling coils, T-type matching network, and the full-bridge rectifier was presented. The importance of the matching network in the overall system performance was demonstrated. Depending on the input resistance of the coupled coils, which is a function of the distance between Tx/Rx coils and being different from the optimum load resistance of the PA, a methodology was proposed for the T-type matching circuit design, where the values for the lumped elements were extracted from the Smith chart analysis. For validation

purposes, the class-E PA with cost-effective IRF640 MOSFET transistor was separately designed and tested, and the complete structure of WPT system was further implemented showcasing its behavior in presence and absence of the proposed T-network at 10 cm and 25 cm. A good agreement was achieved between the analytical and experimental results. The PA efficiency and output power was measured as high as 96.7% and 25.8 W, respectively, for the optimum load value of 9 Ω, which was closely predicted from the theory. Moreover, it was demonstrated that the T-network provides 33% and 12% efficiency increase at 10 cm at 25 cm, respectively. The overall DC output power achieved using a full-bridge rectifier were 21.9 W and 6.8 W at 10 cm and 25 cm, respectively. The working ability of the WPT system was successfully tested to wirelessly light up a 3 W LED at the 25 cm separation distance thanks to the proposed matching network strategy. One perspective would be to store enough energy with a voltage high enough to power sensors including power management circuits.

Declaration of Competing Interest

The authors declare that they have no known competing financial interests or personal relationships that could have appeared to influence the work reported in this paper.

References

[1] Shinohara N. Wireless power transfer via radiowaves. 1st ed. Hoboken, New Jersey: John Wiley & Sons; 2014.
[2] Garnica J, Raul A. Chinga, Lin J, Wireless power transmission: From far field to near field. Proc. IEEE 2013;101:1321–31. https://doi.org/10.1109/JPROC.2013.2251411.
[3] Agrawal DP, Zeng QA. Introduction to wireless and mobile systems. 3th ed. Stamford: Cengage learning; 2015.
[4] Kshatri DB, Shrestha S, Shrestha B. A Brief Overview of Wireless Power Transfer Techniques. Int.J advanced smart convergence 2015;4:1–5. https://doi.org/10.7236/IJASC.2015.4.2.1.
[5] Kim H, Song C, Kim DH, Jung DH, Kim IM, Kim YI, Kim J. Coil design and measurements of automotive magnetic resonant wireless charging system for high-efficiency and low magnetic field leakage. IEEE Trans Microw Theory Techn 2016;64:383–400. https://doi.org/10.1109/TMTT.2015.2513394.
[6] Campi T, Cruciani S, Feliziani M, Maradei F. Magnetic field generated by a 22 KW-85 KHz wireless power transfer system for an EV. In: AEIT Int Annual Conf. Cagliari, Co; 2017.
[7] Koohestani M, Zhadobov M, Ettorre M. Design methodology of a printed WPT system for HF-band mid-range applications considering human safety regulations. IEEE Trans Microw Theory Techn 2016;65:270–9. https://doi.org/10.1109/TMTT.2016.2609931.
[8] Rybicki K, Wojciechowski RM. Analysis and design of a class-E current-driven rectifier for 1 MHz wireless power transfer system. Journal of Electrical Engineering 2019;70:58–63. https://doi.org/10.2478/jee-2019-0008.
[9] Polo J, Hontecillas L, Izquierdo I, Casas O. Micro air vehicles energy transportation for a wireless power transfer system. International Journal of Micro Air Vehicles 2019. https://doi.org/10.1177/1756829319870057.
[10] Jow UM, Ghovanloo M. Design and optimization of printed spiral coils for efficient transcutaneous inductive power transmission. IEEE Trans. Biomed. Circuits Syst. 2007;1:193–202. https://doi.org/10.1109/TBCAS.2007.913130.
[11] Fu W, Zhang B, Qiu D. Study on frequency-tracking wireless power transfer system by resonant coupling. In: 6th International Power Electronics and Motion Control Conference IEEE; 2009. https://doi.org/10.1109/IPEMC.2009.5157857.
[12] Yusop Y, Saat S, Nguang SK, Husin H, Ghani Z. Design of capacitive power transfer using a class-E resonant inverter. Journal of Power Electronics 2016;16:1678–88. https://doi.org/10.6113/JPE.2016.16.5.1678.
[13] Kumar G, Kumar A, Shekhar KS, Bajpai P. Wireless power transfer for Mobile charging applications. Int. Jrnl Research Applied Science Engineering Technology (IJRASET) 2018;6. http://doi.org/10.22214/ijraset.2018.6095.
[14] Choi J, Tsukiyama D, Tsuruda Y, Davila JMR. High-frequency, high-power resonant inverter with egan fet for wireless power transfer. IEEE Trans Power Electron 2017;33:1890–6. https://doi.org/10.1109/TPEL.2017.2740293.
[15] Zhong W, Zhang C, Liu X, Hui SR. A methodology for making a three-coil wireless power transfer system more energy efficient than a two-coil counterpart for extended transfer distance. IEEE Trans Power Electron 2014;30:933–42. https://doi.org/10.1109/TPEL.2014.2312020.
[16] Kazimierczuk MK. RF power amplifiers. 2nd ed. Chichester, West Sussex: Wiley; 2014.
[17] Liu S, Liu M, Yang S, Ma C, Zhu X. A novel design methodology for high-efficiency current-mode and voltage-mode class-E power amplifiers in wireless power transfer systems. IEEE Trans Power Electron 2016;32:4514–23. https://doi.org/10.1109/TPEL.2016.2600268.
[18] Fu M, Yin H, Zhu X, Ma C. Analysis and tracking of optimal load in wireless power transfer systems. IEEE Trans Power Electron 2014;30:3952–63. https://doi.org/10.1109/TPEL.2014.2347071.
[19] Koohestani M, Tissier J, Latrach M. A miniaturized printed rectenna for wireless RF energy harvesting around 2.45 GHz. AEU - Int J Electron Commun 2020;127:153478. https://doi.org/10.1016/j.aeue.2020.153478.
[20] Fu M, Yin H, Liu M, Ma C. Loading and power control for a high-efficiency class-E PA-driven megahertz WPT system. IEEE Trans Industr Electron 2016;63:6867–76. https://doi.org/10.1109/TIE.2016.2582733.
[21] Ahn D, Mercier PP. Wireless power transfer with concurrent 200 KHz and 6.78 MHz operation in a single-transmitter device. IEEE Trans Power Electron 2015;31:5018–29. https://doi.org/10.1109/TPEL.2015.2480122.
[22] Fereshtian A, Ghalibafan J. Impedance matching and efficiency improvement of a dual-band wireless power transfer system using variable inductance and coupling method. AEU-Int J Electron Commun 2020;116:153085. https://doi.org/https://doi.org/10.1016/j.aeue.2020.153085.
[23] Duong TP, Lee JW. Experimental results of high-efficiency resonant coupling wireless power transfer using a variable coupling method. IEEE Microwave Wirel Compon Lett 2011;21:442–4. https://doi.org/10.1109/LMWC.2011.2160163.
[24] Sample AP, Meyer DT, Smith JR. Analysis, experimental results, and range adaptation of magnetically coupled resonators for wireless power transfer.IEEE. Trans Industr Electron 2010;58:544–54. https://doi.org/10.1109/TIE.2010.2046002.
[25] Li Y, Zhang C, Yang Q, Li J, Zhang Y, Zhang X, Xue M. Improved ant colony algorithm for adaptive frequency-tracking control in WPT system. IET Microw Antennas Propag 2017;12:23–8. https://doi.org/10.1049/iet-map.2017.0159.
[26] Luo Y, Yang Y, Chen S, Wen X. A frequency-tracking and impedance-matching combined system for robust wireless power transfer. Int J Antennas Propag 2017. https://doi.org/https://doi.org/10.1155/2017/5719835.
[27] Liu M, Liu S, Ma C. A high-efficiency/output power and low-noise megahertz wireless power transfer system over a wide range of mutual inductance. IEEE Trans Microw Theory Techn 2017;65:4317–25. https://doi.org/10.1109/TMTT.2017.2691767.
[28] Seo DW, Lee JH, Lee HS. Study on two-coil and four-coil wireless power transfer systems using Z-parameter approach. ETRI J 2016;38:568–78. https://doi.org/https://doi.org/10.4218/etrij.16.0115.0692.
[29] Şengül M, Yeşilyurt G. Real frequency design of Pi and T-matching networks with complex terminations. In: IEEE 10th Int Conf Electrical Electron Engineering (ELECO).Co; 2017. p. 1328–31.
[30] Thompson M, Fidler JK. Determination of the impedance matching domain of impedance matching networks. IEEE Trans Circuits Systems I 2004;(51):2098–106. https://doi.org/10.1109/TCSI.2004.835682.
[31] Liu M, Fu M, Ma C. Parameter design for a 6.78 MHz wireless power transfer system based on analytical derivation of class-E current-driven rectifier. IEEE Trans Power Electron 2015;31:4280–91. https://doi.org/10.1109/TPEL.2015.2472565.
[32] Dai X, Li X, Li Y, Hu AP. Impedance-matching range extension method for maximum power transfer tracking in IPT system. IEEE Trans Power Electron 2017;33:4419–28. https://doi.org/10.1109/TPEL.2017.2716968.
[33] Fu M, Tang Z, Liu M, Ma C, Zhu X. Full-bridge rectifier input reactance compensation in megahertz wireless power transfer systems. IEEE PELS Workshop Emerging Tech 2015: Wireless Power (WoW); 1–5. doi: 10.1109/WoW.2015.7132854.
[34] Kee SD, Aoki I, Hajimiri A, Rutledge D. The class-E/F family of ZVS switching amplifiers. IEEE Trans Microw Theory Tech 2003;51:1677–90. https://doi.org/10.1109/TMTT.2003.812564.
[35] Hayati M, Lotfi A, Kazimierczuk MK, Sekiya H. Analysis, design, and implementation of the class-E ZVS power amplifier with MOSFET nonlinear drain-to-source parasitic capacitance at any grading coefficient. IEEE Trans Power Electron 2013;29:4989–99. https://doi.org/10.1109/TPEL.2013.2286160.
[36] Slade B. Notes on designing class-E RF power amplifiers. 2010:1–11.
[37] Shi Y, Zhang Y, Shen M, Fan Y, Wang C, Wang M. Design of a novel receiving structure for wireless power transfer with the enhancement of magnetic coupling. AEU-Int J Electron Commun 2018;95:236–41. https://doi.org/https://doi.org/10.1016/j.aeue.2018.08.033.
[38] Ustun D, Balci S, Sabanci K. A parametric simulation of the wireless power transfer with inductive coupling for electric vehicles, and modelling with artificial bee colony algorithm. Measurement 2020;150:107082. https://doi.org/https://doi.org/10.1016/j.measurement.2019.107082.
[39] Wei W, Kawahara Y, Kobayashi N, Asami T. Characteristic analysis of double spiral resonator for wireless power transmission. IEEE Trans Antennas Propag 2013;62:411–9. https://doi.org/10.1109/TAP.2013.2287521.
[40] Grebennikov A. A high-efficiency transmission-line GaN HEMT class-E power amplifier. High Frequency Electronics 2009;8:16–24.